

## Formation and chemical structure of the Au/Si(111) interface

S. L. Molodtsov,\* C. Laubschat, and G. Kaindl

*Institut für Experimentalphysik, Freie Universität Berlin, Arnimallee 14, D-1000 Berlin 33, Germany*

A. M. Shikin and V. K. Adamchuk

*Institute of Physics, Leningrad State University, Leningrad 198 904, U.S.S.R.*

(Received 26 November 1990; revised manuscript received 11 March 1991)

The formation of the Au/Si(111) interface was investigated by photoemission and partial-electron-yield spectroscopy using synchrotron radiation, as well as by electron-excited Auger-electron spectroscopy. For *n*-type Si(111), the Fermi level is found to shift by 0.43 eV toward the center of the band gap due to band bending at the interface. The chemical structure of the interface depends quite critically on the thickness of the deposited Au layer: for very low Au coverages,  $\Theta < 2 \text{ \AA}$ , Au forms an unreacted ad-layer; in the intermediate range,  $2 \leq \Theta \leq 25 \text{ \AA}$ , a reacted layer with a composition close to  $\text{Au}_3\text{Si}$  is found; in the high-coverage range,  $\Theta > 25 \text{ \AA}$ , the interfacial layer has a sandwich structure, with an unreacted metallic Au phase buried underneath a reacted layer. The critical Au thickness for chemical interaction between Au and Si(111) is explained in terms of the evolving electronic structure of Au with increasing Au coverage.

### I. INTRODUCTION

The formation of interfaces between noble metals and Si has been a topic of widespread interest during the past decade.<sup>1-8</sup> It is mainly based on endeavors to improve the understanding of the electronic and structural properties of these systems for both technological and more fundamental reasons. In particular, the widespread use of such interfaces in electronic devices, like Schottky barriers or Ohmic contacts, serves as a strong incentive for studying their formation and chemical structure.

Interfaces between covalent elemental semiconductors, like Si, and *d*-transition metals represent highly suitable systems for investigating the nature of *p-d* hybridization. Quite different from Ag, which forms a rather abrupt interface with Si,<sup>6</sup> the other *d*-transition metals react chemically with the Si surface, giving rise to alloyed interfaces or even to the formation of chemical compounds in the interfacial layer.<sup>7,8</sup> Among these interfaces, Au/Si(111) has been studied most extensively in the past. Despite the fact that Au and Si are known to form no thermodynamically stable bulk compounds,<sup>1</sup> the Au/Si(111) interface has been found to be reactive, giving rise to the formation of compounds or alloys at the interface.<sup>1,2</sup> Like Ag, bulk Au has almost completely filled *d*-electron states, which are, however, situated closer to the Fermi level ( $E_F$ ) than those of Ag. A study of the origin of reactive interface formation is particularly interesting in the case of Au/Si(111), since it is expected to shed light on the role of noble-metal *d*-states in the interaction with a covalent semiconductor. An additional impetus comes from the recent discovery of superconductivity in Au/Si(111) alloy films.<sup>9</sup>

In previous work, a variety of experimental methods has been applied to investigate Au/Si interfaces providing complementary information on electronic and

structural properties. These include photoemission and Auger-electron spectroscopy,<sup>1-3</sup> low-energy electron diffraction (LEED), inverse photoemission,<sup>10</sup> x-ray-absorption near-edge structure,<sup>9</sup> x-ray standing-wave spectroscopy,<sup>11</sup> and scanning-tunneling microscopy.<sup>12</sup> It is well established by now that for high Au coverages the top layer always contains Si. However, several unsolved problems remain, like the question of the existence of a "critical" Au thickness for Si—Si bonds breaking and forming a reacted Au-Si phase.<sup>5,7</sup> In addition stoichiometry and thickness of the various reacted phases remain unclear as well as the nature of chemical interaction between Au and Si. Moreover, the process of Schottky-barrier formation at the interface requires more detailed investigations. The present study addresses these questions by the use of several complementary experimental methods: core-level and valence-band photoemission (PE), Auger-electron spectroscopy (AES), and partial-electron-yield (PY) spectroscopy.

The paper is organized as follows. After an experimental Sec. II, we present in Sec. III the set of experimental results from core-level PE and Auger-electron spectroscopy. In Sec. IV, the data on valence-band structure are discussed. Section V contains results of partial-electron-yield spectroscopy at the Au  $N_{\text{VI,VII}}$  and Si  $L_{\text{II,III}}$  thresholds. In the final section, Sec. VI, a model for the process of Au/Si(111) interface formation, based on the present results, is described.

### II. EXPERIMENTAL DETAILS

The PE and PY measurements were performed at the Berliner Elektronenspeicherring für Synchrotronstrahlung (BESSY) using a toroidal-grating monochromator (TGM-1) and a hemispherical electron-energy analyzer. The overall-system resolution in PE was  $\approx 0.2$

eV [full-width at half maximum (FWHM)] allowing a determination of binding-energy (BE) changes with an accuracy of  $\pm 0.03$  eV. In a separate experimental setup, a modified cylindrical-mirror analyzer with a resolution of 0.2% was employed for Auger-electron spectroscopy, using a 3-keV primary electron beam with  $\pm 0.5$ -eV amplitude modulation. The base pressure in both experimental chambers was  $\approx 10^{-10}$  Torr.

Pieces of *n*-doped Si(111) wafers were used as substrates, with the cleaning procedure performed in UHV pressures of typically  $10^{-10}$  Torr; the wafers were not pretreated by etching. The Si(111) surface was cleaned by Ar-ion sputtering followed by flash annealing at  $\approx 900^\circ\text{C}$ . These cleaning cycles were repeated until no traces of C or O could be detected in the AES or valence-band PE spectra and sharp  $7\times 7$  LEED patterns were observed. Au was evaporated from a gold bead melted on a thin tungsten wire; such an evaporation source allows one to keep the pressure in the experimental chamber during Au deposition in the  $10^{-10}$ -Torr range. The Au coverage was monitored by a quartz microbalance. Since the aim of the present work was to study interface formation at room temperature, the Au layers were not subsequently annealed. Previous investigations using AES, low-energy electron-loss spectroscopy, and scanning electron microscopy had shown that Au deposited under these conditions on Si(111) grows in a layer-by-layer mode, while deposition at higher substrate temperatures ( $\approx 400^\circ\text{C}$ ) leads to agglomeration.<sup>13,14</sup> Following each Au deposition, Si 2*p* and Au 4*f* PE and PY spectra as well as Si(*L**V**V*) and Au(*N**V**V*) Auger spectra were recorded. Before a new set of spectra was taken, the Si(111) substrate was again Ar-ion sputtered and characterized by LEED, AES, and photoelectron spectroscopy (PES). To reach a clean surface, several sputtering cycles were usually performed until the clean surface was finally annealed.

Si 2*p* and Au 4*f* core-level PE spectra were taken with synchrotron radiation at photon energies of  $h\nu=115$  and 130 eV, respectively; these photon energies were selected in order to establish almost identical photoelectron kinetic energies in the region of maximum surface sensitivity. Valence-band PE spectra were studied with a photon energy of  $h\nu=40$  eV. The recorded spectra were least-squares fitted with Lorentzian lines (Si 2*p* and valence-band spectra) or Doniach-Sunic lines (Au 4*f* spectra) convoluted by a Gaussian to account for finite experimental resolution. In order to achieve relatively high surface sensitivity in the PY measurements, only electrons with kinetic energies in the region of minimum sampling depth, given by the "universal curve," were monitored.

Si(*L**V**V*) and Au(*N**V**V*) Auger spectra were taken in the  $dN/dE$  mode. In order to obtain the local valence-band partial density of Si *sp* states from the line shape of the Si(*L**V**V*) Auger spectrum, a deconvolution of the spectrum was performed employing the global inversion method, which is based on the discrete Fourier transform.<sup>15</sup> To isolate the Si(*L**V**V*) spectra from the experimental spectra for interfaces with various Au coverages, Au(*N**V**V*) Auger spectra were subtracted. Distortions in the line shape, caused by secondary electrons originating

from PE and Auger processes, were corrected for by subtracting an integral scattering background.

### III. CORE-LEVEL PE AND AUGER-ELECTRON SPECTRA

#### A. Discussion of experimental spectra

In Fig. 1(a), Si 2*p* core-level PE spectra for various Au coverages on Si(111) are displayed. The bottom spectrum from a freshly cleaned Si(111) surface is composed of two spin-orbit-split final-state doublets from bulk (dashed) and surface (dash-dotted) atoms. From a least-squares fit of the spectrum, a surface core-level shift of  $-0.48$  eV is derived, in close agreement with a previous result.<sup>16</sup> For a Au coverage of  $0.5 \text{ \AA}$ , a redistribution of the relative intensities of bulk and surface components is observed, resulting from a partial relaxation of the electronic struc-

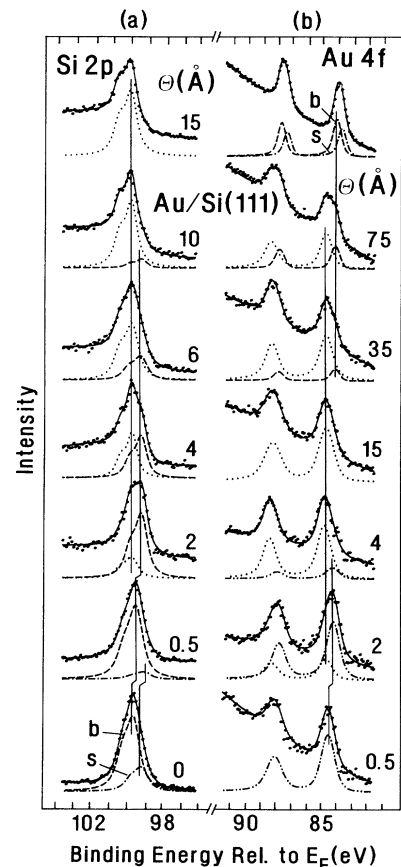


FIG. 1. (a) Si 2*p*,  $h\nu=130$  eV, and (b) Au 4*f*,  $h\nu=115$  eV, core-level PE spectra of the Au/Si(111) interface as a function of Au coverage  $\Theta$ . The solid lines through the data points represent the results of least-squares fits. The dashed subspectra stem from (a) the unreacted bulk Si substrate or (b) bulk Au metal, while the dotted components originate from a reacted phase. Surface and bulk features are marked by *s* and *b*, respectively. Dashed-double-dotted lines display the signal from submonolayer nonreacted Au.

ture of surface atoms. The reacted components (dotted), which appears at higher Au coverages ( $\Theta \geq 2 \text{ \AA}$ ), is not observed at a coverage of only  $0.5 \text{ \AA}$  of Au. This means that the nature of interaction between Au and Si(111) depends on the thickness of the Au deposit. With increasing Au coverage, the spectra are shifted to lower binding energies. This is a consequence of band bending, i.e., of a movement of the Fermi level toward the center of the band gap, away from its original position in bulk *n*-type Si close the conduction-band minimum. The amount of band bending can be derived in a direct way from the binding energy of the bulk Si  $2p_{3/2}$  component shown in Fig. 1(a); it reaches a value of  $-0.43 \text{ eV}$  for  $\Theta \approx 2 \text{ \AA}$ . Further deposition of Au does not cause any additional change in BE of the bulk Se  $2p_{3/2}$  component.

For coverages  $\Theta \geq 2 \text{ \AA}$ , a reacted component (dotted) appears in the spectra indicating the formation of a new phase. The Si  $2p_{3/2}$  BE of this reacted phase is found to be independent of Au coverage, and  $0.61 \text{ eV}$  higher than that of bulk Si. With further deposition, the reacted component becomes dominant, and for coverages beyond  $\approx 10 \text{ \AA}$  it completely defines the spectra. From  $\Theta \approx 15 \text{ \AA}$  on, no further changes in the Si  $2p$  core-level PE spectrum are noted. This means that even for high Au coverages, a reactive Au-Si layer is always observed on the surface of the interfacial layer. The chemical shift  $\Delta E_B$  of the Si  $2p_{3/2}$  level of the reacted phase should be measured relative to the Si  $2p_{3/2}$  BE,  $E_B^i$ , of an intrinsic Si crystal (with  $E_F$  in the center of the band gap). Assuming  $E_B^i = 99.30 \text{ eV}$  (relative to  $E_F$ ),<sup>4</sup> a value of  $\Delta E_B = E_B^{\text{Au/Si}} - E_B^i = 0.65 \text{ eV}$  is obtained for  $\Theta \geq 2 \text{ \AA}$ .

Au  $4f$  core-level PE spectra for various Au coverages on Si(111) and for a thick layer of metallic Au deposited on a nonreactive W substrate are shown in Fig. 1(b). All spectra were least-squares fitted by a superposition of doublets with Doniach-Sunic line shapes. Decomposition of the top spectrum, taken from metallic Au, defines two spin-orbit-split components with BE's of  $84.07 \text{ eV}$  (bulk, dashed) and  $83.70 \text{ eV}$  (surface dash-dotted) for the  $4f_{7/2}$  PE line. The difference in BE represents the surface core-level shift,  $\Delta_{\text{SCS}} = -0.37 \text{ eV}$ , in agreement with a previous result.<sup>17</sup> The least-squares fit result for the case of metallic bulk Au is used as a reference for the fits of the other spectra. For the highest Au coverages studied,  $\Theta \geq 23 \text{ \AA}$ , the spectra can be described by a superposition of two doublets. One of them (dashed) is assigned to unreacted metallic Au. The relative weight of the second dotted component, which is shifted to high BE, increases with decreasing Au coverage, dominating the spectrum for  $\Theta = 15 \text{ \AA}$ . A comparison of these observations with the Si  $2p$  spectra shown in Fig. 1(a) suggests that this dotted component originates from the reacted phase in the Au/Si(111) interfacial layer. It exhibits a Au  $4f$  chemical shift of  $0.66 \text{ eV}$  to higher BE relative to bulk metallic Au. The growth in relative intensity of the PE signal from unreacted metallic Au with increasing Au deposition for  $\Theta \geq 23 \text{ \AA}$  displays the formation of an unreacted metallic Au phase in the interfacial layer. This phase, however, seems to be formed beneath a reacted Au-Si layer, since the PE signal from the reacted phase remains stronger than that from metallic Au even for the higher Au cover-

ages studied ( $\Theta \geq 75 \text{ \AA}$ ).

For low Au coverages,  $\Theta \leq 4 \text{ \AA}$ , analysis of the Au  $4f$  PE spectra results again in two subspectra (dotted and dash-double-dotted). While the dotted subspectrum is at the BE of the reacted components, the second subspectrum is situated close to the one from metallic bulk Au [Fig. 1(b)]. When proceeding from  $0.5$  to  $2 \text{ \AA}$  Au coverage, the latter component follows the shift of the Si  $2p$  core level to lower BE as expected upon metallization of the adlayer.<sup>18</sup> The dominant character of the dash-double-dotted subspectrum for submonolayer and monolayer Au coverages illustrates the existence of a critical Au coverage for the beginning of Au-Si chemical interaction on Si(111); this critical coverage is found to be  $\approx 2 \text{ \AA}$ , in agreement with our conclusion from the analysis of Si  $2p$  PE intensities.

We have performed theoretical estimates for the chemical shifts of core-level PE BE's on the basis of the Miedema, Boom, and de Boer scheme.<sup>19</sup> In both cases studied, the observed chemical shifts of the reacted phase differ from those calculated for  $\text{Au}_3\text{Si}$  by only  $0.03 \text{ eV}$ . For comparison, the differences between the calculated  $\Delta E_B$  values for the Au  $4f$  lines in the case of  $\text{Au}_3\text{Si}$  and phases like  $\text{Au}_2\text{Si}$  or  $\text{Au}_4\text{Si}$  amount to about  $0.15 \text{ eV}$ . We note that the stoichiometric composition of  $\text{Au}_3\text{Si}$  is close to the eutectic point in the Au-Si binary phase diagram.<sup>20</sup>

Figure 2 shows the evolution of the Si(LVV) and

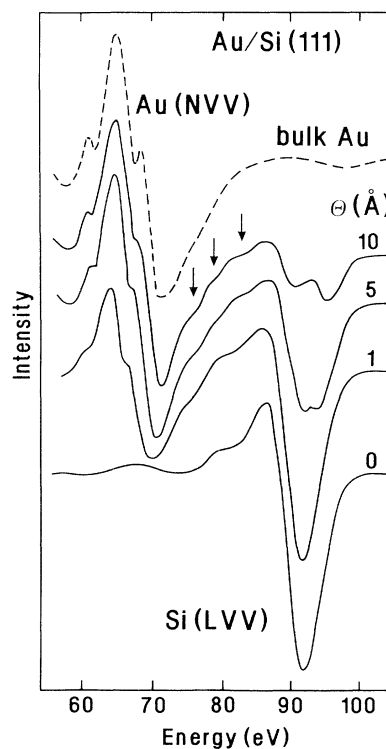


FIG. 2. Si(LVV) and Au(NVV) Auger-electron spectra of Au/Si(111) for various Au coverages  $\Theta$  (solid lines). The dashed spectrum was taken from a thick metallic Au film deposited on a nonreactive W substrate.

Au(*NVV*) Auger spectra as a function of Au coverage on Si(111). The top spectrum (dashed) stems from bulk metallic Au. A gradual increase of the intensity of the Au(*NVV*) spectrum is observed with increasing Au deposition, while the shape of the spectrum does not change significantly. Simultaneously, a decrease in Si(*LVV*) intensity is observed. The Si(*LVV*) peak broadens with increasing Au coverage, which leads for  $\Theta \geq 4$  Å to a splitting into two components at  $\approx 90$  and  $\approx 94.5$  eV, respectively. This splitting is caused by a change in the occupied local density of states due to Au-Si chemical interaction. We note that additional spectral features, marked by vertical arrows, are observed in the Auger spectra at kinetic energies between 70 and 90 eV.

### B. Analysis of spectral intensities

Figure 3 displays the relative intensities of the various PE subspectra and Auger spectra as a function of Au coverage for Au/Si(111). Here, the PE spectral intensities are defined as peak areas normalized to the storage-ring electron-beam current; the AES intensities are taken as peak-to-peak amplitudes normalized to the current of the electron gun. Figure 3(a) shows that the relative

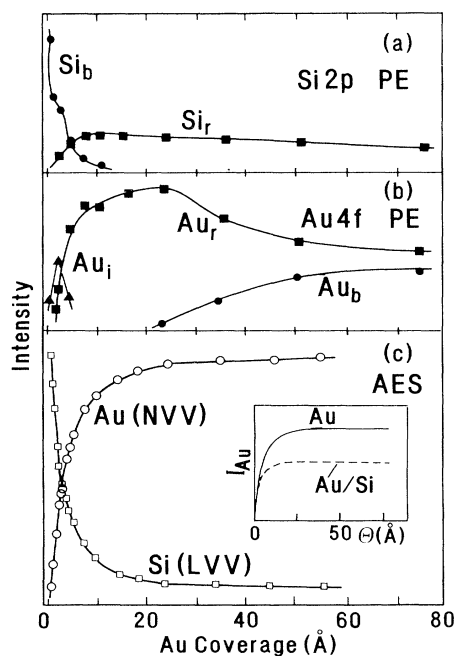


FIG. 3. Spectral intensities as a function of Au coverage on Si(111) for (a) Si 2*p* PE, (b) Au 4*f* PE, and (c) Si(*LVV*) and Au(*NVV*) Auger signals. For the PE intensities, closed squares are used to denote the reacted component: closed circles, the Si-bulk or the metallic-Au phases; and solid triangles, the submonolayer of nonreacted Au on Si(111). In (c) open circles (open squares) represent the intensities of Au(*NVV*) [Si(*LVV*)] Auger signals. The inset in (c) gives the dependence of the normalized Au(*NVV*) Auger intensity for Au deposited on the nonreacted substrate (solid curve) and for Au/Si(111) (dashed curve), respectively (see text).

weight of the Si 2*p*<sub>3/2</sub> PE component from the unreacted substrate decreases monotonically with Au coverage, becoming negligible for  $\Theta \geq 15$  Å. A small shoulder is observed in the intensity-versus-coverage curve for  $0.5 \leq \Theta \leq 2$  Å. The reacted Si 2*p*<sub>3/2</sub> component displays a broad intensity maximum between  $\approx 6$  and  $\approx 25$  Å, with its relative weight decreasing slowly with increasing Au coverage. It is striking that a Si 2*p*<sub>3/2</sub> PE signal can still be monitored for Au coverages as high as  $\approx 75$  Å.

The intensity of the reacted component in the Au 4*f*<sub>3/2</sub> PE spectrum exhibits also a broad maximum at similar coverages as the reacted Si 2*p* PE component [Fig. 3(b)]. At higher coverages, a smooth decay toward a saturation value, reached at a coverage of  $\approx 60$  Å, is found; the intensity in the saturation region is only about half of that in the maximum. At a coverage of  $\approx 20$  Å, the growth of an unreacted metallic Au phase begins, as can be inferred from the coverage dependence of the Au 4*f*<sub>7/2</sub> PE component originating from such a metallic phase [Au<sub>b</sub> curve in Fig. 3(b)]. While the Au<sub>b</sub> intensity increases steeply in the low-coverage range (for  $\Theta < 50$  Å), it saturates at higher coverages at a value substantially smaller than that of the reacted component and also than that of the bulk component from a thick Au film. By comparing the PE intensity of this unreacted metallic Au phase for  $\Theta = 75$  Å,  $I_{75 \text{ Å}}^b$ , which is assumed to be buried underneath a Au<sub>3</sub>Si layer, with the sum of intensities of the bulk ( $I_m^b$ ) and surface ( $I_m^s$ ) components in the 4*f*<sub>7/2</sub> core-level PE spectrum of a thick Au film, the thickness of the reacted surface layer may be estimated. With an attenuation length of 4 Å, derived from the slope of the Si<sub>b</sub>( $\Theta$ ) curve in Fig. 3(a), an experimental ratio  $I_{75 \text{ Å}}^b / (I_m^b + I_m^s) = 0.35$  is found corresponding to approximately one monolayer of Au<sub>3</sub>Si on the surface of the Au-Si interfacial layer.

Figure 3(b) reveals that a PE signal from submonolayer nonreacted Au is only observed for Au coverages less than  $\approx 4$  Å. The increase in intensity of the respective PE signal [Au<sub>i</sub> in Fig. 3(b)] with increasing  $\Theta$ , observed for  $0.5 \leq \Theta \leq 2$  Å, is brought to an abrupt stop at  $\Theta \approx 2-3$  Å; this signals again the beginning of chemical interaction between Au and Si.

In Fig. 3(c), the intensity of the Si(*LVV*) AES spectrum is shown as a function of Au coverage; it decreases monotonically with  $\Theta$  reaching a saturation value for  $\Theta \geq 30$  Å. Again, from the slope of the curve we obtain an attenuation length of  $\approx 4.5$  Å, which agrees with the mean free path of Auger electrons expected in case of a layer-by-layer growth mode. On the other hand, a continuous growth of the Au(*NVV*) Auger intensity is observed for  $\Theta$  up to  $\approx 50$  Å. The inset in Fig. 3(c) shows the Au(*NVV*) intensities normalized to the backscattering factor for Au/Si(111) (dashed curve) and for Au deposited on a nonreactive substrate (solid curve). From a comparison of these two intensities we conclude that the amount of Si on the surface of the Au/Si(111) interfacial layer corresponds to approximately one monolayer of Au<sub>3</sub>Si.<sup>21</sup>

In the following, we summarize the conclusions from a joint analysis of intensities of the various components in

the core-level PE and AES spectra of Au/Si(111). Essentially three stages may be distinguished in the process of interface formation.

(i) Low-coverage deposition of Au on Si(111),  $\Theta < 2 \text{ \AA}$ , does not lead to a breaking of Si—Si bonds or interdiffusion of Si and Au atoms.

(ii) The intermediate-coverage region from  $\approx 2$  to  $\approx 25 \text{ \AA}$  is characterized by strong interdiffusion of Au and Si and the formation of a reacted Au-Si phase with approximate stoichiometry  $\text{Au}_3\text{Si}$ .

(iii) The high-coverage region,  $\theta > 25 \text{ \AA}$ , is governed by the formation of an unreacted metallic Au phase beneath approximately a monolayer of reacted  $\text{Au}_3\text{Si}$ .

In this way, the Au/Si(111) interface is characterized by a “sandwich” structure. This is in accord with the results of a previous study of Au/Si(111) by AES depth-profile analysis.<sup>22</sup>

#### IV. VALENCE-BAND ELECTRONIC STRUCTURE

A study of the electronic structure of occupied and unoccupied states close to  $E_F$  provides additional information on the nature of chemical interaction between Au and Si. These valence-band states are directly involved in the formation of chemical bonds between Au and Si. For a study of the Au 5*d* states, PE measurements in the valence-band region with photon energy of  $h\nu = 40 \text{ eV}$  were performed.

A set of valence-band spectra for various Au depositions on Si(111), taken with  $h\nu = 40 \text{ eV}$ , is shown in Fig. 4. One first notices that the spectra are dominated by Au 5*d* states for all Au depositions studied. The splitting of the two 5*d*-derived spectral branches increases with Au coverage, reflecting an increasing interaction between neighboring Au atoms and reaches a final value of 2.2 eV at  $\Theta \approx 15 \text{ \AA}$ .

For high Au coverages ( $\Theta \geq 23 \text{ \AA}$ ), a shoulder *A* at the low-binding-energy side of the 5*d*<sub>5/2</sub> derived branch is observed. Such a shoulder has been noticed before and was assigned to the formation of a Au-Si compound.<sup>3</sup> However, the present study is not supporting such an assignment, since it clearly shows that  $\text{Au}_3\text{Si}$  is already formed for Au coverages as low as 15  $\text{ \AA}$ . In addition, the shape of the valence-band spectrum observed for  $\Theta = 15 \text{ \AA}$  agrees quite well with the results of a density-of-states calculation for  $\text{Au}_3\text{Si}$ .<sup>2</sup> Instead, we notice here that shoulder *A* appears in the valence-band spectrum at a coverage of  $\Theta \geq 23 \text{ \AA}$ , i.e., when the formation of an unreacted metallic Au phase buried in the interfacial layer begins. The spectra for  $\Theta = 23$  and 75  $\text{ \AA}$  in Fig. 4 were accordingly least-squares fitted to a superposition of two subspectra, defined by the spectral shapes of bulk gold (dashed) and of  $\text{Au}_3\text{Si}$  (dotted), respectively. The solid curves through the data points in the 23- and 75- $\text{ \AA}$  spectra of Fig. 4 are the results of this special analysis, with the subspectra and their relative intensities also given. The quality of these fits demonstrates that shoulder *A* should be assigned to the signal from an unreacted metallic gold phase in the interfacial layer.

Figure 5 shows the spectral region close to the Fermi level both for a coverage of 15- $\text{ \AA}$  Au and for bulk Au

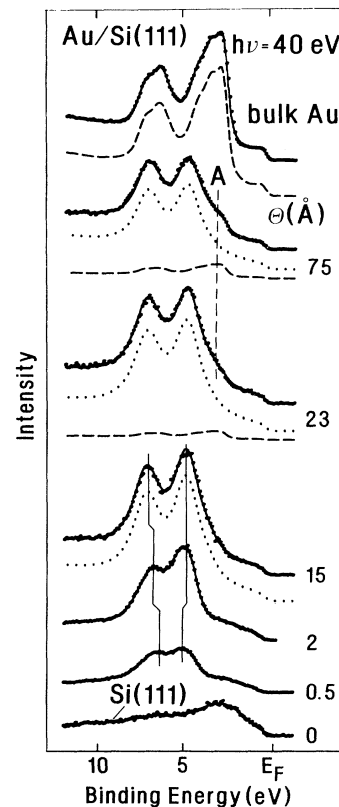


FIG. 4. Valence-band PE spectra of the Au/Si(111) interface for various Au coverage  $\Theta$ . The bottom spectrum represents clean Si(111), while the top one was taken from a thick layer of Au metal. The spectra for high Au coverages,  $\Theta = 23$  and 75  $\text{ \AA}$ , are composed of two subspectra, one from a reacted phase (dotted) and the other one from an unreacted metallic gold (dashed).

metal in more detail. As is evident from this figure, the spectral intensity close to  $E_F$  is smaller for the Au/Si system than for Au metal. This may be due to the observed narrowing of the 5*d* band and reflects a decrease of a density of *d* states at  $E_F$  in Au/Si(111) as compared to Au metal, in agreement with the results of our PY measurements (see Sec. V). Alternatively, a decrease in the par-

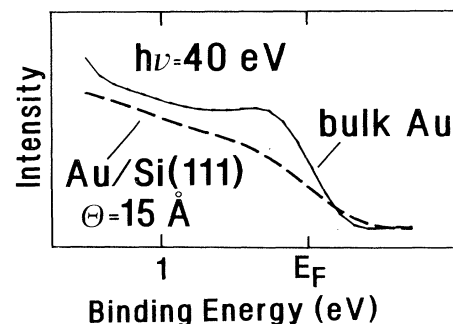


FIG. 5. Valence-band PE spectra close to  $E_F$  in detail: dashed, 15- $\text{ \AA}$  Au/Si(111); solid, bulk Au. The spectra intensities are normalized with respect to equal photon flux.

tial density of  $s$  states may also be discussed.

To gain further information on changes of the local density of states at the Si site during the process of interface formation, we have studied Si( $LVV$ ) AE spectra in more detail. It is well known that Si( $LVV$ ) Auger spectra represent a self-convolution of the local occupied valence-band density of states. Figure 6 displays the results of such a self-deconvolution of the Auger spectra for various Au coverages on Si(111). The absolute energy scale in Fig. 6 was obtained from a comparison of the spectrum of clean Si(111) with the respective valence-band PE spectrum. A more direct energy calibration from the Auger spectra is complicated by uncertainties in the relaxation energy. The results in Fig. 6 show that the local density of states undergoes significant changes in the Au/Si(111) interfacial layer as a function of Au coverage. For coverages  $\Theta \geq 4 \text{ \AA}$ , essentially three peaks are observed in the density of states: two well-separated features at BE's of  $\approx 1 \text{ eV}$  and  $\approx 5 \text{ eV}$ , respectively, and a third peak around 13 eV. A comparison with the bottom spectrum from clean Si(111) reveals a considerable redistribution of Si  $sp$  states due to hybridization with the metal  $d$  states.<sup>2</sup> We relate the 1- and 5-eV peaks to hybridized Au  $5d$ /Si  $3p$  bands, while the 13-eV feature may be assigned to Si  $s$ -derived states.

### V. PARTIAL-ELECTRON-YIELD SPECTRA

Information on partial densities of unoccupied states and their variation may also be derived from PY studies.

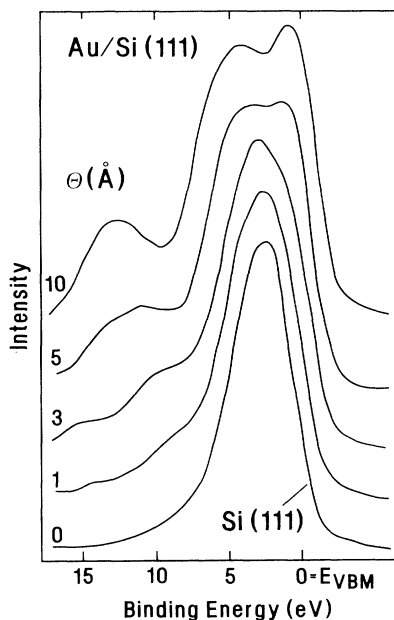


FIG. 6. Partial density of Si  $sp$ -derived valence-band states for Au/Si(111) as a function of Au coverage  $\Theta$ . The curves were obtained from self-deconvolution of Si( $LVV$ ) Auger spectra. Binding energy refers to the valence-band maximum ( $E_{VBM}$ ).

In the present work, such PY spectra of Au/Si(111) were recorded in the regions of the Au  $N_{VI,VII}$  and Si  $L_{II,III}$  thresholds. In order to achieve a relatively high surface sensitivity and to avoid the effects of primary-photoelectron lines passing through the PY window, secondary electrons with kinetic energies of 30 and 50 eV, respectively, were recorded for the Si and Au thresholds.

Figure 7 shows typical PY spectra of Au/Si(111) for various Au coverages in the region of (a) the Au  $N_{VI,VII}$  and (b) the Si  $L_{II,III}$  thresholds. The peaks at the  $N_{VI}$  and  $N_{VII}$  thresholds of Au [Fig. 7(a)] correspond to  $4f_{5/2} \rightarrow 5d_{3/2,5/2}$  excitation (at  $\approx 89 \text{ eV}$ ) and  $4f_{7/2} \rightarrow 5d_{5/2}$  excitations (at  $\approx 86 \text{ eV}$ ), respectively. The observation of absorption structures at the Au  $N_{VI,VII}$  thresholds reveals that even in Au metal, the  $5d$  shall is not completely filled, in agreement with the results from band-structure calculations predicting about 0.4  $d$  holes per atom (.0283 holes of  $d_{5/2}$  and 0.118 holes of  $d_{3/2}$  character).<sup>23</sup> The weak relative intensity of the peak at  $N_{VI}$  is striking; it may be caused by many-body effects in the excitation process as discussed previously.<sup>24</sup> In the following, we will therefore only discuss the structure at  $N_{VII}$  observed in all PY spectra of Au/Si(111). The dashed curve in the inset of Fig. 7(a) represents the  $N_{VII}$ -peak intensity as a function of Au coverage on Si(111), normalized to the number of absorbing Au atoms; this was achieved via the Au  $4f$  core-level PE intensity taking the different surface sensitivities of PE and PY methods

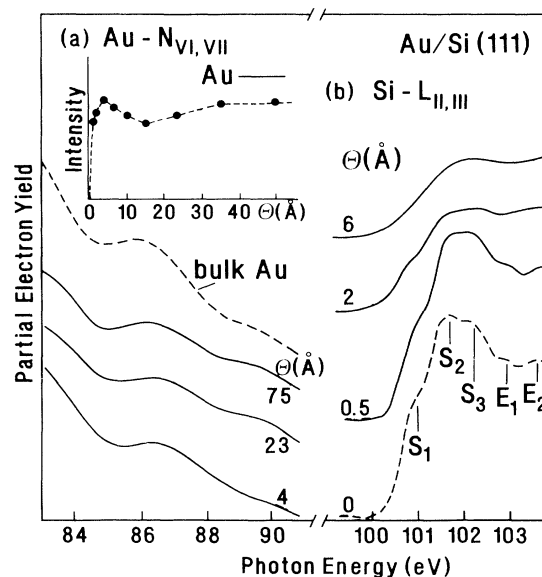


FIG. 7. PY spectra of Au/Si(111) at (a) the Au  $N_{VI,VII}$  and (b) the Si  $L_{II,III}$  thresholds for various gold coverages  $\Theta$ . The dashed spectrum in (a) was recorded from bulk Au metal, while the dashed spectrum in (b) was obtained from the clean Si(111) substrate. The inset in (a) shows the white-line intensity at the Au  $N_{VII}$  threshold normalized to the corresponding Au  $4f_{7/2}$  PE-line intensity as a function of Au coverage. The solid horizontal bar represents the Au  $N_{VII}$  intensity for bulk Au.

into account. The normalized-intensity curve reflects therefore the variation of the unoccupied local partial  $d$  density of states at  $E_F$  as a function of Au coverage. After an initial steep increase, the  $d$  density of states decreases in the coverage range from  $\approx 4$  to  $\approx 15$  Å, reflecting the intense chemical interaction between Au and Si.

It is interesting to note, that in spite of the large bandwidth in the reacted phase (see Fig. 4), the number of unoccupied  $d$  states is obviously smaller than for submonolayer coverages. This may be explained by a distinct dispersive behavior of the different hybridized bands: For submonolayer coverages as well as for Au metal, hybridization takes place between  $d$  and  $s$  states, and the larger dispersion of the  $s$  states leads to a wide spread of  $d$  character. In the case of the reacted phase, however,  $p$ - $d$  hybrids are dominant, and the weaker dispersion of the Si-derived  $p$  states diminishes the spread of  $d$  character.

For Au coverages exceeding  $\approx 15$  Å, a renewed increase is observed due to the formation of an unreacted metallic Au phase in the interfacial layer. Note, that for all Au coverages studied, the normalized  $N_{\text{VII}}$ -peak intensity stays well below that observed for bulk Au metal [horizontal bar in Fig. 7(a)]. This is in good agreement with the behavior of the density of states close to  $E_F$  observed by valence-band PE spectroscopy (Fig. 5).

PY spectra at the  $L_{\text{II,III}}$  threshold of Si are presented in Fig. 7(b), both for clean Si(111) and for Au/Si(111) with three different Au coverages. The five features marked by vertical bars in the spectrum of clean Si(111) agree well with previous electron-energy-loss spectroscopy (EELS) and inverse-photoemission observations:<sup>25,26</sup>  $S_1$  to  $S_3$  are assigned to excitations into unoccupied surface states, while  $E_1$  and  $E_2$  reflect transitions into unoccupied bulk states. In the case of Au/Si(111), the surface-state features become less pronounced with increasing Au coverage, while the bulk features gain in relative weight. For  $\Theta \geq 6$  Å, the PY spectra turn rather structureless due to an additional signal from the reacted layer, which is shifted to higher energies.

## VI. THE PROCESS OF Au/Si(111) INTERFACE FORMATION

The present work shows clearly that the formation of interfaces between Au and Si(111) is strongly influenced

by chemical interaction between Au and Si. Essentially two models for the Au-Si chemical interaction have been discussed up to now.

(i) Chemical interaction from the very beginning of Au deposition.<sup>27</sup> This concept, however, is not supported by other observations.<sup>7,28</sup>

(ii) Existence of a critical thickness of Au for the formation of a metallic Au layer, with the weakly bound conduction electrons screening the Si—Si bonds.<sup>29</sup> This model, however, is unable to explain the different behavior of the isoelectronic Ag/Si system, which is known to be nonreactive for all coverages.

The present results suggest that the process of Au-Si interaction is mainly governed by the evolution of the electronic structure of Au with increasing Au coverage. At low coverages, when the width of the Au  $5d$  band is small, we are in a situation similar to that of Ag/Si, where the energy separation of the metal-derived  $d$  states from Si-derived  $p$  states close to  $E_F$  is large enough to suppress  $pd$  hybridization. At higher Au coverages, the increasing interaction between neighboring Au atoms leads to a broadening of the  $d$  band and, consequently, to an increasing energy overlap of the  $d$  states with Si-derived  $p$  states. This suggests the existence of a critical coverage, where one arrives at a situation similar to that encountered in transition-metal/Si systems. There, the degeneracy of Si  $p$  and metal  $5d$  states favors the formation of hybrid bonds causing chemical reaction at the interface. Thus, in the framework of this certainly oversimplified picture, the existence of a critical thickness for chemical interaction is readily understood. A more elaborate model, however, should also consider the role of  $s$  states.

## ACKNOWLEDGMENTS

This work was partially supported by the Bundesminister für Forschung und Technologie, Contract No. 05-413AXI/TP2. One of the authors (S.L.M.) thanks the Freie Universität Berlin for financial support and hospitality. Valuable discussions with D. A. Shirley are gratefully acknowledged.

\*Permanent address: Institute of Physics, Leningrad State University, Leningrad 198 904, U.S.S.R.

<sup>1</sup>L. Braicovich, I. Abbati, J. N. Miller, I. Lindau, S. Schwarz, P. R. Skeath, C. Y. Su, and W. E. Spicer, *J. Vac. Sci. Technol.* **17**, 1005 (1980).

<sup>2</sup>O. Bisi, C. Calandra, L. Braicovich, I. Abbati, G. Rossi, I. Lindau, and W. E. Spicer, *J. Phys. C* **15**, 4707 (1982).

<sup>3</sup>K. Hricovini, J. E. Bonnet, B. Carriere, J. P. Deville, M. Hanbücken, and G. Le Lay, *Surf. Sci.* **211/212**, 630 (1989).

<sup>4</sup>J.-J. Yeh, J. Hwang, R. Cao, K. A. Bertness, and I. Lindau, *J.*

*Vac. Sci. Technol. A* **6**, 1557 (1988).

<sup>5</sup>M. Iwami, M. Kubota, T. Koyama, H. Tochiwara, and Y. Murata, *Phys. Rev. B* **38**, 1047 (1988).

<sup>6</sup>J. Derrien, G. Le Lay, and F. Salvan, *J. Phys. Lett.* **39**, L287 (1978).

<sup>7</sup>V. K. Adamchuk, I. V. Lyubinetskii, and A. M. Shikin, *Pis'ma Zh. Tekh. Fiz.* **12**, 1056 (1986) [*Sov. Tech. Phys. Lett.* **12**, 436 (1986)].

<sup>8</sup>M. Hanbücken and G. Le Lay, *Surf. Sci.* **168**, 122 (1986).

<sup>9</sup>Y. Jeon, N. Jisrawi, G. Liang, F. Lu, M. Croft, W. L. McLean,

- D. L. Hart, N. G. Stoffel, J. Z. Sun, and T. H. Geballe, *Phys. Rev. B* **39**, 5748 (1989).
- <sup>10</sup>J. M. Nicholls, F. Salvan, and B. Reihl, *Phys. Rev. B* **34**, 2945 (1986).
- <sup>11</sup>S. M. Durbin, L. E. Berman, B. W. Battermann, and J. M. Blakely, *J. Vac. Sci. Technol. A* **3**, 973 (1985).
- <sup>12</sup>J. Nogami, A. A. Baski, and C. F. Quate, *Phys. Rev. Lett.* **65**, 1611 (1990).
- <sup>13</sup>G. Le Lay, *Surf. Sci.* **132**, 169 (1983).
- <sup>14</sup>P. Perfetti, S. Nannarone, F. Patella, C. Quaresima, M. Capozzi, A. Savoia, and G. Ottaviani, *Phys. Rev. B* **26**, 1125 (1982).
- <sup>15</sup>V. K. Adamchuk and A. M. Shikin, *J. Electron Spectrosc. Relat. Phenom.* **52**, 103 (1990).
- <sup>16</sup>F. J. Himpsel, P. Heimann, T.-C. Chiang, and D. E. Eastman, *Phys. Rev. Lett.* **45**, 1112 (1980).
- <sup>17</sup>P. H. Citrin, G. K. Wertheim, and Y. Baer, *Phys. Rev. Lett.* **41**, 1425 (1978).
- <sup>18</sup>M. Prietsch, M. Domke, C. Laubschat, and G. Kaindl, *Phys. Rev. Lett.* **60**, 436 (1988).
- <sup>19</sup>A. R. Miedema, R. Boom, and F. R. De Boer, *J. Less Common Metals* **41**, 283 (1985).
- <sup>20</sup>R. P. Anantatmula, A. A. Johnson, S. P. Gupta, and R. J. Horylev, *J. Electron. Mater.* **4**, 445 (1975).
- <sup>21</sup>V. K. Adamchuk, S. I. Fedoseenko, and A. M. Shikin, *Poverkhnost U.S.S.R* **12**, 43 (1985).
- <sup>22</sup>V. K. Adamchuk and I. V. Lyubinetskii, *Zh. Tekh. Fiz.* **56**, 1853 (1986) [*Sov. Phys.—Tech. Phys.* **31**, 1108 (1986)].
- <sup>23</sup>L. F. Mattheiss and R. E. Dietz, *Phys. Rev. B* **22**, 1663 (1980).
- <sup>24</sup>S. P. Kowalczyk, L. Ley, R. L. Martin, F. R. McFeely, and D. A. Shirley, *Faraday Discuss. Chem. Soc.* **60**, 7 (1975).
- <sup>25</sup>H. H. Farrell, F. Stucki, J. Anderson, D. J. Frankel, G. J. La Peyre, and M. Levinson, *Phys. Rev. B* **30**, 721 (1984).
- <sup>26</sup>F. J. Himpsel and Th. Fauster, *J. Vac. Sci. Technol. A* **2**, 815 (1984).
- <sup>27</sup>L. Braicovich, C. M. Garner, P. R. Skeath, C. Y. Su, P. W. Chye, I. Lindau, and W. E. Spicer, *Phys. Rev. B* **20**, 5131 (1979).
- <sup>28</sup>M. Iwami, T. Terada, H. Tochiara, M. Kubota, and Y. Murata, *Surf. Sci.* **194**, 115 (1988).
- <sup>29</sup>K. Okuno, T. Ito, M. Iwami, and A. Hiraki, *Solid State Commun.* **34**, 493 (1980).